Polymer Degradation and Stability 217 (2023) 110543

Contents lists available at ScienceDirect

Polymer Degradation and Stability

journal homepage: www.journals.elsevier.com/polymer-degradation-and-stability

# Processability and reprocessability maps for vitrimers considering thermal degradation and thermal gradients

D. Sanchez-Rodriguez [b,*], S. Zaidi [b], Y. Jahani [a], A. Ruiz de Luzuriaga [c], A. Rekondo [c], P. Maimi [a], J. Farjas [b], J. Costa [a]

[a] AMADE - Analysis and Advanced Materials for Structural Design, Polytechnic School, University of Girona, C/ Universitat de Girona 4, E-17003, Girona, Spain
[b] GRMT Materials Research Group and Thermodynamics, Polytechnic School, University of Girona, C/ Universitat de Girona 4, E-17003, Girona, Spain
[c] CIDETEC, Basque Research and Technology Alliance (BRTA), Po. Miramón 196, 20014, Donostia-San Sebastián, Spain

ARTICLE INFO

*Keywords:*
Processability maps
Reprocessability maps
Vitrimers
Aromatic disulfides
Epoxy resins
Thermal stability

ABSTRACT

A lack of fundamental knowledge about the kinetic mechanisms governing the processing and reprocessing of vitrimers forces a trial-and-error procedure to be adopted when choosing treatment conditions. In this work, we develop diagrams to be used as a straightforward tool to decide the curing and thermoforming parameters of vitrimers. The thermal stability of a disulfide containing epoxy has been evaluated by means of thermal analysis methods. By characterizing the kinetics of the curing and decomposition of the resin through a model-free kinetic method, we have been able to generate an intuitive processability map based on Time-Temperature-Transformation plots. The resulting chart allows for the optimum curing conditions that will avoid degradation to be identified. A similar chart for reprocessability has been obtained by considering the exchange kinetics of the characteristic stress relaxation behavior of vitrimers. Furthermore, we have incorporated into the diagrams criteria to determine the critical thickness below which a tolerable thermal gradient is not exceeded. Our diagrams have been experimentally validated, thus proving to be a useful and valid tool for rapid decision-making situations.

## 1. Introduction

To improve energy efficiency in transport, using composite materials as lightweight structural components is a generalized trend in industries such as aerospace and the automotive industry [1,2]. Within structural composites, thermoset matrices have been the most popular choice to date [3] as they provide good mechanical properties and good adhesion to the fiber. However, thermosetting resins cannot be recycled [4] and, in the current climate-emergency context, this is a major drawback that has led to promising alternatives now being considered [5]. Among the top options are the so-called vitrimers; a new type of resin based on the covalent adaptable network (CAN) concept that offers a good balance between sustainability and performance [6–8]. Vitrimers are covalently cross-linked polymers and at service temperatures they behave like thermosets. The distinctive feature of these novel eco-friendly resins is that external stimuli such as light or temperature can trigger the topological rearrangement of their covalent network, thus, making them remoldable and self-healing and, therefore, repeatedly recyclable and repairable [9]. Of all the vitrimers, it is the epoxy-based ones that excel in the availability of monomers and ease of synthesis which, in turn, facilitates their scalability in an industrial setup [10]. In particular, epoxy vitrimer composites incorporating reversible crosslinks based on aromatic disulfides offer excellent mechanical properties and their use in industrial applications is straightforward [11–13].

As with any other resin, one of the key points that will ultimately determine the commercial success of aromatic disulfide-containing epoxy vitrimers is curing time. Long curing times increase manufacturing costs and limit production to low-to-medium-volume batches. However, pushing the curing processes to shorten production times may lead to a sudden and accelerated increase in the reaction rate that raises the sample temperature locally by tens or even hundreds of degrees. This phenomenon, known as thermal runaway, is self-sustained, resulting in zero control over the process treatment. Given the occurrence of a thermal runaway, overheating can be so high that it may even exceed the degradation temperature of the resin, thus affecting the mechanical properties of the material [14]. Esposito et al.,

* Corresponding author.
*E-mail address:* daniel.sanchez@udg.edu (D. Sanchez-Rodriguez).

https://doi.org/10.1016/j.polymdegradstab.2023.110543
Received 3 August 2023; Received in revised form 14 September 2023; Accepted 23 September 2023
Available online 23 September 2023

studied the effect of curing overheating on the mechanical behavior of fiber-reinforced epoxy laminates [15]. The study reported interlaminar shear strength losses of up to 13 % due to overheating. This could be a particularly critical issue in vitrimers using aromatic disulfide hardeners since their thermal stability is slightly lower than that of other commercial hardeners commonly used for curing thermosets [16].

Many models attempting to describe the kinetics of the curing reaction of thermosetting resins have been proposed. The most popular is undoubtedly that proposed by Kamal [17–19] based on the Šesták–Berggren equation [20] which accounts for the autocatalytic nature of the reaction. By coupling these models to the heat transport equations, many researchers have numerically analyzed the temperature evolution of a resin during curing. For instance, William et al. [21] numerically analyzed the particular case of a graphite/epoxy composite with the aim of obtaining uniform and controlled conversion degrees in autoclave-processes. The authors targeted an optimum degree of conversion, less than 100 %, at which the best compromise between $T_g$ and mechanical properties at room temperature is obtained. Their analysis led them to propose a cycle where overheating did not exceed the programmed temperature by more than a few degrees, thus preventing the mechanical properties from being impaired. Besides, their simulations revealed that, for thick samples subjected to high heating rates, curing could even result in an incipient thermal degradation of the resin. Michaud et al. [22], when trying to address the problem arising from the formation of thermal gradients during resin curing, proposed an empirical autocatalytic model to phenomenologically describe the curing kinetics of thick-section RTM composites. More recently, Leister et al. [23] adapted the Kamal–Sourour curing model to fit the experimental data of an Araldite epoxy resin. They took into account the dependence of the degree of cure on system parameters such as the thermal conductivity or specific heat of the resin. The model was implemented in a finite element program and solved for the three-dimensional case; roughly reflecting the experimentally measured evolution of the temperature within the sample. Simulations based on realistic numerical models such as Leister's are a preventive tool to anticipate possible unwanted overheating. Nevertheless, this type of models requires hours of computation and do not provide a criterion that allows optimizing the curing cycle beyond a pure trial-and-error approach.

From a practical point of view, models leading to analytical expressions are undoubtedly much more useful for rapid decision-making situations. Previously, we determined an analytical relationship that readily provided a criterion for avoiding significant temperature gradients forming within a sample in thermal analysis experiments [24]. Our analysis accounted for heat propagation and the heat released by an exothermic reaction in samples heated at a constant rate. Recently, we further developed the model to account for isothermal conditions and low enthalpic reactions [25]. The resulting analytical expression is especially appealing for predicting thermoset resin overheating during curing.

The thermal stability of vitrimers is also at risk during reprocessing. Thermoforming vitrimers requires temperatures high enough to activate the exchange reactions, however, at high temperatures this recombination process competes with the thermal degradation of the polymer. Just as with thermoplastics when they are repeatedly melted down for recycling [26], thermal degradation might lead to detrimental changes in the properties of reprocessed vitrimers. Such changes would result in a significant loss of material performance that may end up disabling it for certain applications. Therefore, for thermoforming processes one needs to understand the dynamic stress relaxation behavior of the vitrimers. Some aromatic disulfide-containing epoxy vitrimers have shown remarkably rapid relaxation times without the need to incorporate catalysts [27]. Ruiz de Luzuriaga et al., provided a methodology to adjust the dynamic properties of these types of vitrimers to match the requirements of different processing technologies. In their work, the success of the proposed thermoforming cycles was evaluated on the basis of the storage modulus drop of the post-processed material. Still, there is no formal criterion to guarantee thermal stability during reprocessing beyond tests.

An intuitive way to assess the feasibility of a process is to graphically describe the effect of the main processing variables, such as cycle time, temperature, or sample thickness. Based on their own thermochemical model, Gayot et al., developed processing maps for the polymerization of thick metracrylic films [28]. The authors coupled curing kinetics to the critical conditions for void formation due to local monomer boiling. Likewise, our overheating prediction [25], together with a curing kinetic study and a degradation kinetic study, would allow us to develop a processing map for our epoxy vitrimers cured with aminophenyl disulfide hardeners. In this work, we build diagrams that provide an accurate picture of the conditions under which complete curing of the epoxy-based vitrimer can be achieved whilst avoiding degradation. To that end, we will develop Time-Temperature-Transformation (TTT) plots, as these are especially useful for optimizing thermally driven processes. This type of graphical representation has been previously applied to epoxy thermosets to optimize curing cycles [19,29]. TTT diagrams are even helpful in predicting the reversible nature of polymers based on dissociative covalent adaptive networks, such as those based on dynamic Diels-Alder linkages [30]. To complete the processability map, we will characterize the evolution of the glass transition temperature, $T_g$, as a function of epoxy conversion. Likewise, we develop a similar diagram for reprocessability, accounting for stress relaxation and degradation kinetics, thus resulting in a powerful tool for the optimization of thermoforming and self-healing cycles while assuring the thermal stability of the vitrimer.

## 2. Materials and methods

### 2.1. Materials

The formulation of the epoxy-based vitrimer was supplied by Cidetec (Donostia-San Sebastian, Spain), which holds the patent for it. The formulation is the same as that presented by Ruiz de Luzuriaga et al., in the vitrimer labeled as V2 in their previous work [11]. It consists of commercially available functional epoxy groups DGEBA (Araldite LY1564) and a new (also commercially available) hardener with dynamic cross-linking based on aromatic disulfide species (4-Aminophenyl disulfide). For the mixing, the NH equivalents were set as 1.1 per epoxy group.

### 2.2. Calorimetric experiments

For the calorimetric experiments, we have used the Q2000 apparatus of TA. The heat flow calibration of the apparatus in the entire temperature range of interest was carried out using sapphire discs. The experiments were performed under a constant flow of nitrogen of 50 mL/min. Prior to each DSC run, a small amount of uncured sample (4–6 mg) was sealed into a standard aluminum pan. Curing kinetics was analyzed under non-isothermal conditions (Section 2.5) from DSC measurements taken at a series of constant heating rates, ranging from 1.25 °C/min to 20 °C/min, over a temperature range from 0 to 300 °C. A number of uncured samples were cured to different target degrees in accordance with non-isothermal predictions based on an isoconversional kinetic analysis (Section 2.6) [31]. Following standard procedure, their $T_g$ was determined as the midpoint of the extrapolated initial and final transition temperatures [32]. The specific heat capacity (Cp) of the vitrimer was obtained by following the ASTM standard method E-1269 [33] (Fig. 1). A $T_{g\infty}$ of 133 °C was determined from the transition change observed in the evolution of heat capacity.

### 2.3. Thermal degradation study

Thermogravimetric analysis of the fully-cured resin has been carried

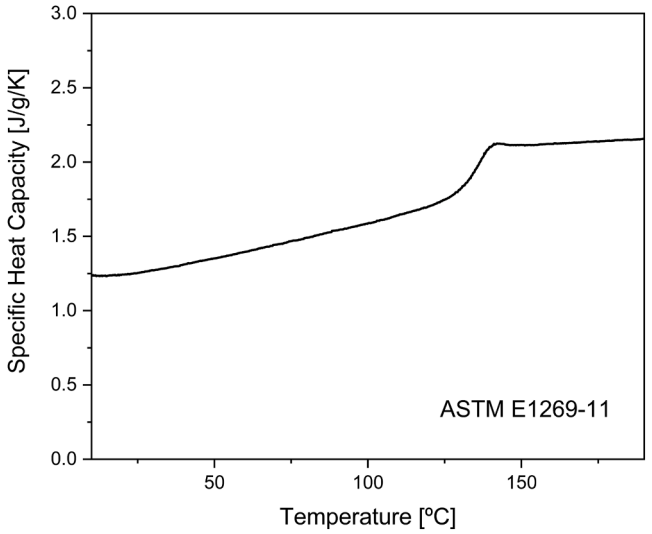


**Fig. 1.** (single column fitting image) - Evolution of the specific heat capacity.

out in air using a Mettler Toledo thermo-balance, model TGA/DSC1. Samples were heated at a series of constant rates, ranging from 1.25 °C/min to 20 °C/min, under a dynamic atmosphere (flow rate of 55 ml/min of carrier gas and 15 ml/min of the protective gas). Experiments were conducted at atmospheric pressure and uncovered 70-μl-$Al_2O_3$ pans were used. *In-situ* TG-FTIR was performed to monitor the evolution of the volatiles during the decomposition of the samples heated at 20 °C/min. To do so, the TG was coupled to the gas cell (Bruker ALPHA model) through a 40-cm-long steel tube kept at 200 °C. Interpretation of the MS spectra of the volatiles was made according to NIST reference spectra.

### 2.4. Thermal conductivity test

A self-made Poensgen apparatus was used to measure the thermal conductivity, k, of the fully cured vitrimer. A 5 mm thick plate of cured vitrimer was heated under a controlled heat flux until a constant temperature difference was reached. The thermal conductivity was calculated from the one-dimensional Fourier's law expression, assuming the heat losses through the thickness of the plate to be negligible. Following this method, a k of 0.136 W/(K·J) was obtained at 50 °C.

### 2.5. Isoconversional kinetic analysis

Both resin curing and resin degradation exhibit complex reaction kinetics. Because of this, determining accurately the kinetic parameters is a challenging task when attempting to apply model-fitting methods. Conversely, methods based on phenomenological models are more versatile [10.1002/pen.10777]. For instance, isoconversional methods allow the kinetic parameters to be determined without the need to reveal the specific mechanism governing the reaction and have been successfully applied to adjust the curing kinetics of thermoset resins [34–38]. Among isoconversional methods, the so-called differential and advanced ones account for the dependence of kinetic parameters on the degree of transformation, α. These methods are based on the assumption that for a given α, the transformation rate is a function of temperature, T, and degree of transformation, α ($0 \leq \alpha \leq 1$):

$$\left[\frac{d\ln(d\alpha/dt)}{dT^{-1}}\right]_{\alpha} = -\frac{E_\alpha}{R} \tag{1}$$

where $E_\alpha$ is the apparent activation energy for this degree of transformation and R is the ideal gas constant. The integration of Eq. (1) leads to:

$$\frac{d\alpha}{dt} = A_\alpha f(\alpha) e^{-E_\alpha/(RT)} \tag{2}$$

Eq. (2) can be used to calculate the evolution of the reaction once $E_\alpha$ and $A_\alpha f(\alpha)$ have been determined. To that purpose we used Friedman's differential isoconversional method which can be derived by the linearization of Eq. (2) [39].

$$ln\left[\left(\frac{d\alpha}{dt}\right)_{T_{\alpha,i}}\right] = ln[A_\alpha f(\alpha)] - \frac{E_\alpha}{RT_{\alpha,i}} \tag{3}$$

To determine the kinetic parameters for a given α, $E_\alpha$ and $A_\alpha f(\alpha)$, several experiments were performed at different heating rates $\beta_i$ ($\beta \equiv dT/dt$). Then, for each heating rate $d\alpha/dT|_{\alpha,i}$ and $T_{\alpha,i}$ are determined. Notice that, for a certain value of α, the term $ln[A_\alpha f(\alpha)]$ is constant and the left-hand side of Eq. (2), $ln\left[\beta_i\left(\frac{d\alpha}{dT}\right)_{T_{\alpha,i}}\right]$, shows a linear dependence on the reciprocal temperature. For this linear relationship, $E_\alpha/R$ and $Af(\alpha)$, have been obtained from the slope and the y-intercept, respectively.

### 2.6. Predicting the evolution of solid-state transformations

By applying Friedman's method, the evolution of the kinetic parameters with the degree of transformation is obtained as a series of N discrete sets of values, $E_{\alpha,j}$ and $[A_\alpha f(\alpha)]_j$, where the step employed for the discretization of α(t) is $\alpha_{j-1} = 1/(N - 1)$.

Farjas and Roura [31,40] have developed a prediction method that can be applied to an arbitrary temperature program. The dependence of temperature on time is discretized into constant time intervals, $\Delta t$, so that $t_k = k\,\Delta t$ where $k$ is a natural number and $T_k = T(t_k)$. The method is derived directly from Eq. (2) by replacing the differentials by increments:

$$\alpha_{k+1} = \alpha_k + A_{\alpha_k} f(\alpha_k) exp\left(-\frac{E_{\alpha k}}{RT_k}\right)\Delta t \tag{4}$$

Here, $E_{\alpha,k}$ and $[A_\alpha f(\alpha)]_k$. are determined by an interpolation algorithm [41] from the discrete sets of values $E_{\alpha,j}$ and $[A_\alpha f(\alpha)]_j$.

Following Farjas and Roura's approach [31,40], in this manuscript the kinetic evolutions have been determined directly from the time integration of the transformation rate. This methodology has been applied both to predict the kinetics of curing and decomposition under isothermal conditions, and to predict the degree of curing in samples treated under dynamic conditions (Experiments performed to study the evolution of $T_g$ with the degree of curing).

### 2.7. Overheating criteria

Due to the exothermic nature of the curing reaction and the relatively low thermal conductivity of thermosets, overheating and even thermal runaway can occur when a sample exceeds a critical thickness, depending on the thermal history. Thermal runaway occurs when heat dissipation cannot compensate for heat generation. Below this critical thickness, heat dissipation equals heat generation and the system reaches a steady state, this is the so-called subcritical state [42,43]. Still, the formation of temperature gradients in the subcritical state leads to non-uniform curing and even matrix degradation and delamination [15, 44–46]. Recently, we have experimentally and numerically explored the formation of thermal gradients within the thickness of thin laminates under isothermal curing conditions [25]. To do so, we considered a flat plate geometry and we took into account heat generation and heat propagation. For the boundary conditions, we assumed that one side of the laminate is in perfect thermal contact with a mold, while on the other side heat transport is governed by thermal convection. This is a reasonable assumption for curing resins since at typical processing temperatures the contribution of thermal radiation is negligible. Our

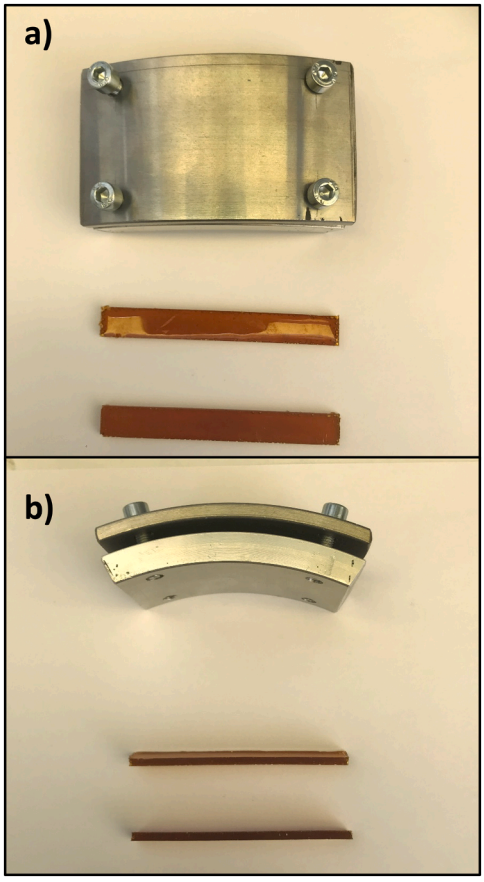


**Fig. 2.** Accessory and coupons for the thermoforming experiments.

analysis led to establishing an analytical expression for the critical laminate thickness, $w_c$, related to a given tolerated overheating, $\Delta T_{max}$:

$$w_c = w_o\left[2-\left(1+0.63\left[h\frac{w_0}{k}\right]^{1.2}\right)^{-1}\right]\left[1+1.6\frac{c}{q}\Delta T_{max}-1.1\left(\frac{c}{q}\Delta T_{max}\right)^2+2.3\left(\frac{c}{q}\Delta T_{max}\right)^3\right], \quad (5)$$

where,

$$w_{c,0}=\sqrt{\delta_{c,0}\frac{k}{\rho q}\frac{RT_m^2}{A}\frac{}{E_a}e^{E_a/RT_m}} \quad and \quad \delta_{c,0}=2e^{-\theta_{Max}}\ \mathrm{arcosh}^2\left(e^{\theta_{Max}/2}\right), \quad \theta_{Max}=E_a\frac{\Delta T_{Max}}{RT_m^2} \quad (6)$$

and c is the specific heat capacity, q is the enthalpy of the reaction, $T_m$ is the mold temperature and $h$ is the effective convective coefficient.

Besides, we also determined the maximum allowable overheating before the reaction kinetics develop into a thermal runaway [47]:

$$\Delta T_{Max,c}=1.18684\frac{RT_m^2}{E_a} \quad (7)$$

The critical thickness for a thermal runaway to occur was then derived by simply combining Eqs. (5) and (7).

In this work, we have used these relationships to define the maximum thickness below which we can ensure not exceeding a tolerable overheating. To apply these criteria, all physical parameters were measured, albeit except for the effective convective coefficient, h, which could only be roughly estimated and was taken to be 70 W/(m$^2$K), a commonly accepted value in laminate curing simulations [15,48].

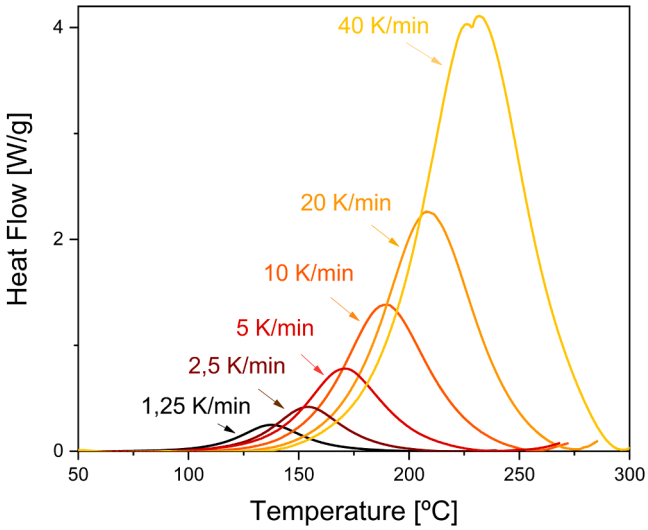


**Fig. 3.** Non-isothermal cure behavior of the resin obtained from DSC experiments performed at different heating rates.

### 2.8. Thermoforming experiments

To assess the thermoforming capability of the vitrimer, two coupons were fully cured and tested. The specimens were flat shaped laminates with length, width, and thickness of 80, 10 and 3 mm, respectively. Each sample was heated in a liquid silicone bath at 155 °C for different times forcing them to remain bent at a constant curvature during the treatment. For this purpose, we built an accessory consisting of two concentric metal curved segments between which the specimen is placed (Fig. 2.a, and Fig. 2.b). By means of screws, it is possible to apply pressure to the specimen to force it to bend and adopt the curvature of the tooling. The inner and outer radii of the deformed sample are approximately 100 and 103 mm, respectively. The final curvature of the samples, once cold and out of the tooling, is used to evaluate the reshaping capacity of the vitrimer.

## 3. Results and discussion

### 3.1. Curing

The DSC curves for the curing of the epoxy vitrimer heated at rates ranging from 1.25 to 20 K/min are shown in Fig. 3. As expected for thermally activated processes, the peak temperature, Tp, shifts to higher temperatures and the peak becomes wider with increasing heating rates [49]. Table 1 summarizes the enthalpy of the reaction determined from the peak area, with values ranging from 425 to 364 J/g. Note that, immediately after the peak the DSC signal slightly rises and extends to temperatures above 250 °C. This heat flow signal corresponds to the onset of the resin's thermal decomposition and evidences that, for heating rates higher than 10 K/min, thermal degradation is overlapping the final curing stages. Thus, only those experiments performed at rates of 1.25, 2.5, 5 and 10 °C/min have been considered for determining the

**Table 1**
The peak temperatures and the heats of reaction at different heating rates.

| β (°C/min) | Tp (°C) | ΔH (J/g) |
|---|---|---|
| 1.25 | 137.4 | 415 |
| 2.5 | 154.2 | 414 |
| 5 | 170.7 | 425 |
| 10 | 188.9 | 409 |
| 20 | 208.3 | 364 |
| 40 | 231.3 | 374 |

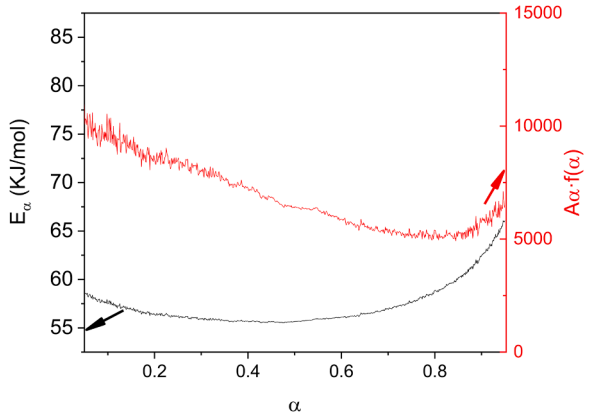


**Fig. 4.** Activation energy, Eα, (Left-side axe) and A(α) f(α) (Right-side axe) as a function of curing degree obtained from Friedman's isoconversional method.

enthalpy, thus resulting in 415.8 ± 6 J/g.

Based on the experiments of Fig. 3 performed up to a heating rate of 10 °C/min, the kinetics governing curing have been analyzed using Friedman's isoconversional method. The evolution of the kinetic parameters, $E_\alpha$ and $A_\alpha f(\alpha)$, with the degree of conversion is depicted in Fig. 4. $E_\alpha$ exhibits values in the region of 55 –70 kJ/mol which are in agreement with those commonly obtained for epoxy-amine systems [19,29]. Up to an approximately 50 % degree of transformation, the apparent activation energy has a rather flat evolution, fluctuating between 55 and 57 kJ/mol. Once the halfway point of the curing process is passed, $E_\alpha$ increases steadily up to completion. These two well-differentiated regions in the evolution of $E_\alpha$ indicate that curing is a complex process. The flat evolution stage could indicate that this region is dominated by the reaction of primary amines with the epoxy groups. The increase in activation energy may well denote the time at which the secondary amines produced start reacting with another epoxy group which yields a tertiary amine, or to the low mobility of longer chains [50,51]. A further explanation could be provided by the fact that, at high conversion, curing is slowing down due to diffusion limitations related to the gelation of the epoxy network [38,52–54].

### 3.2. Vitrification

The build-up of crosslinking upon the reaction of epoxy groups with the hardener is accompanied by an increase in $T_g$. This relationship is well described by the DiBenedetto equation [55] (Eq. (8)) which is the most common way to model $T_g$ changes with the degree of cure [21,56,57].

$$\frac{(T_g - T_{g0})}{(T_{g\infty} - T_{g0})} = \frac{\lambda\alpha}{(1-(1-\lambda)\alpha)}, \tag{8}$$

where $T_{g,0}$ and $T_{g,\infty}$ are, respectively, the transition temperatures of the uncured and fully-cured resin. As for λ, this is a parameter that lies between 0 and 1 which is used to fit the experimental data. Fig. 5 shows the evolution of Tg for a series of samples cured to different degrees. The glass transition ranges from −26 °C, for an uncured sample, up to 133 °C

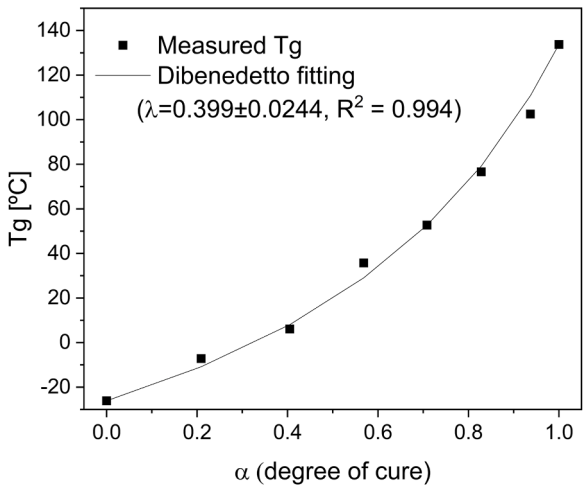


**Fig. 5.** Evolution of the glass transition temperature, Tg, with the degree of curing obtained from DSC measurements.

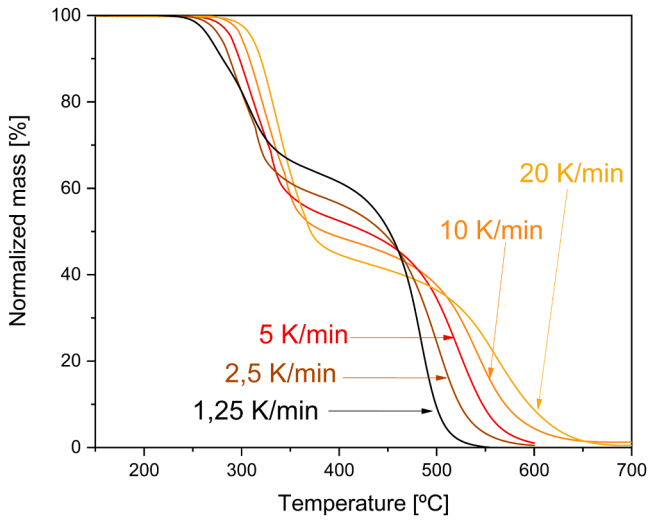


**Fig. 6.** Non-isothermal degradation behavior of the fully-cured resin obtained from TG experiments performed at different heating rates in $N_2$.

at the maximum degree of crosslinking. The experimental data has been fitted following Eq. (8) obtaining a λ value of 0.399±0.024 with R squared equal to 0.994.

### 3.3. Thermal degradation

The mass evolution curves resulting from the thermal decomposition of the fully-cured vitrimer when heated at different rates show that decomposition takes place in two stages (Fig. 6). The onset of the first stage, which defines the stability of the resin, increases along with the heating rate from approximately 250 to 300 °C over the range of experimental conditions investigated. The two stages are not independent processes since the degree of transformation after the first dTG peak clearly depends on the heating rate.

The produced volatiles have been monitored by an FTIR coupled to the TG, revealing that the first stage corresponds to the thermal degradation of the resin while the second stage is related to oxidative combustion. Among the foremost volatiles detected over the course of the low-temperature peak, 4-Isopropylphenol (one of the main products of the thermal degradation of Bisphenol-A Diglycidyl Ether) stands out. It is also important to note the detection of sulfur dioxide; unambiguously attributable to the decomposition of the disulfide hardener. Thus, these

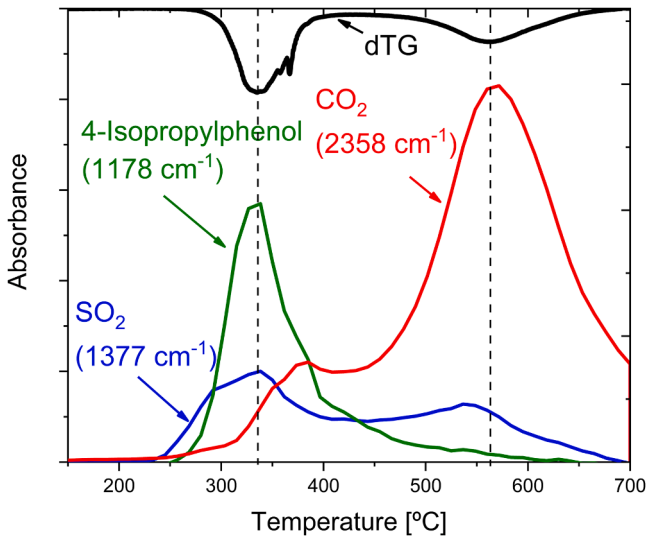


**Fig. 7.** TG-FTIR of the decomposition of the fully-cured epoxy vitrimer heated at 20 °C/min in air.

two compounds permit the thermal stability of the two building blocks constituting the studied vitrimer to be compared. We have traced the release of these two volatiles by tracking the infrared light absorbed at their main characteristic absorption frequency. In particular, we focused on tracking the most intense absorption peaks of their FTIR patterns. (1178 and 1377 $cm^{-1}$ for 4-Isopropylphenol and $SO_2$, respectively). By superimposing the resulting evolutions (Fig. 7), we conclude that the thermal stability of the resin is primarily undermined by the stability of the hardener. Upon breaking the hardener, the backbone of the resin decomposes shortly thereafter, and the two mechanisms of degradation are then coupled to the point of simultaneous occurrence. The peaks of evolution of both 4-Isopropyl phenol and $SO_2$ match the maximum transformation rate of the first process (Fig. 7). The second decomposition stage is largely dominated by the characteristic release of $CO_2$ gas (monitored absorption frequency of 2358 $cm^{-1}$) from the combustion of carbon-containing molecules. At this stage, 4-isopropylphenol is no longer detected as it is not stable at such high temperatures. On the other hand, the evolution of sulfur dioxide still follows that of the dTG curve.

We used the Friedman isoconversional method to characterize the thermal decomposition kinetics of the epoxy resin systems from the curves in Fig. 6. Due to the non-applicability of isoconversional methods

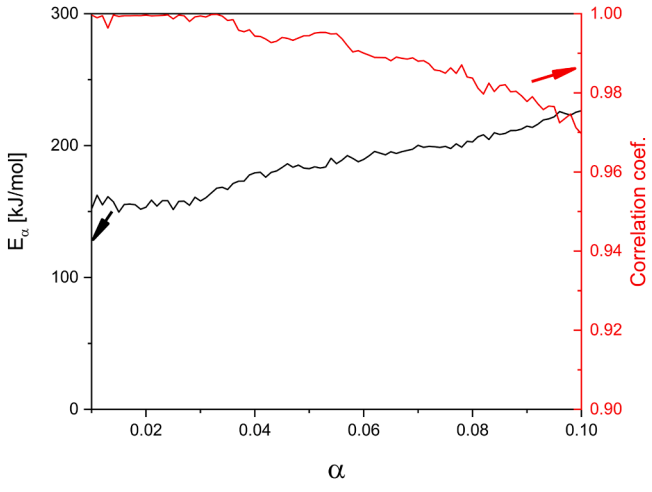


**Fig. 8.** Apparent activation energy as a function of curing degree obtained from Friedman's isoconversional method. Right-side axe shows the correlation coefficient of the method.

to the two separate steps of the decomposition, (because they are not independent processes), both steps have been analyzed as a unique transformation. However, considering the purpose of this work, only the evolution of the kinetic parameters during the early stages of the decomposition have been of interest in assessing the stability of the vitrimer. Therefore, Fig. 8 only shows the evolution of the apparent activation energy up to a transformation degree of 10 %. As shown in the figure, $E_\alpha$ increases steadily with the degree of transformation from an initial 150 kJ/mol to about 220 kJ/mol at $\alpha = 10$ %. In the analyzed range, the method used to calculate $E_\alpha$ shows correlation coefficients close to one.

### 3.4. Processing map

The time required to reach a certain degree of cure under constant temperature conditions has been predicted from the kinetic parameters obtained by the Friedman isoconversional analysis as described in Section 2.6. The black lines in Fig. 9.a show the time required to reach a 90 %, 95 % and 100 % degree of cure for isothermal processing cycles ranging from 70 to 250 °C. Analogously, the kinetic analysis of the decomposition yielded time-temperature-dependent lines accounting for thermal stability. By overlaying both kinetic processes in the same TTT diagram, it is possible to define the maximum processing temperature that guarantees a desired extent of crosslinking while keeping degradation below a tolerable limit. From Fig. 9.a, it can be concluded that, for the studied vitrimer, complete curing is not attainable at temperatures above 215 °C without exceeding a degradation of more than 0.1 %. Besides, from the intersection of the curing and tolerated degradation lines, the minimum processing time is also defined. To continue with the example where the degradation bar is as low as 0.1 %, it is not feasible to fully cure the resin in less than 600 s.

While this analysis sets the limits of the upper processing temperature range, the lower boundary is set by the phenomenon of vitrification. It is reasonable to assume that the rate of curing in the glassy state is negligible at constant temperature [57]. Therefore, we considered the reaction to stop progressing when $T_g$ matches the processing temperature. Taking this point into consideration, the dotted portion of the isoconversional lines show the temperature range where our kinetic analysis is no longer valid for predicting the evolution of cure. The vitrification line has been added to the same TTT processing diagram to facilitate the identification of the maximum degree of cure achievable at temperatures below $T_{g,\infty}$. Hence, from Fig. 9.a it can be noted that, it would not be convenient to treat our epoxy resin below 100 °C if our target is to achieve curing degrees higher than 90 %. From the combination of all three kinetic processes, (i.e., curing, degradation and vitrification), a powerful and intuitive map results in which an optimal window of processing conditions for the vitrimer can be identified.

Yet, a very important ingredient is missing from this scenario: geometry. Ignoring sample thickness, the diagram would fail to address the inherent problems caused by thermal gradients along the thickness of the sample. Inhomogeneities in mechanical properties, residual stresses causing warpage [58] or even uncontrolled degradation of the resin, are some of the common issues of concern. From Eq. (5), one can calculate the maximum thickness above which a tolerable temperature gradient will not be exceeded during processing. The solution is not time-dependent, so we have included an independent diagram in (Fig. 9.b) to account for the sample thickness. Two solid green lines have been added as criteria for the maximum processable thickness if thermal gradients are to be avoided. The light green line sets the limit for an overheating of 5 °C, while the dark green line marks the limit for 10 °C. It must be highlighted that these conditions are obtained by neglecting convective heat losses ($h = 0$ in Eq. (6)). Therefore, this condition would be useful to set a lower limit when preparing thin plates by infusion. For the case of a plate that is heated from one side inside an open mold, we have considered $h = 70$ W/($m^2$K) [15,48], plotted as dashed lines in the same figure. As we pointed out in Section 2.7, there is a maximum

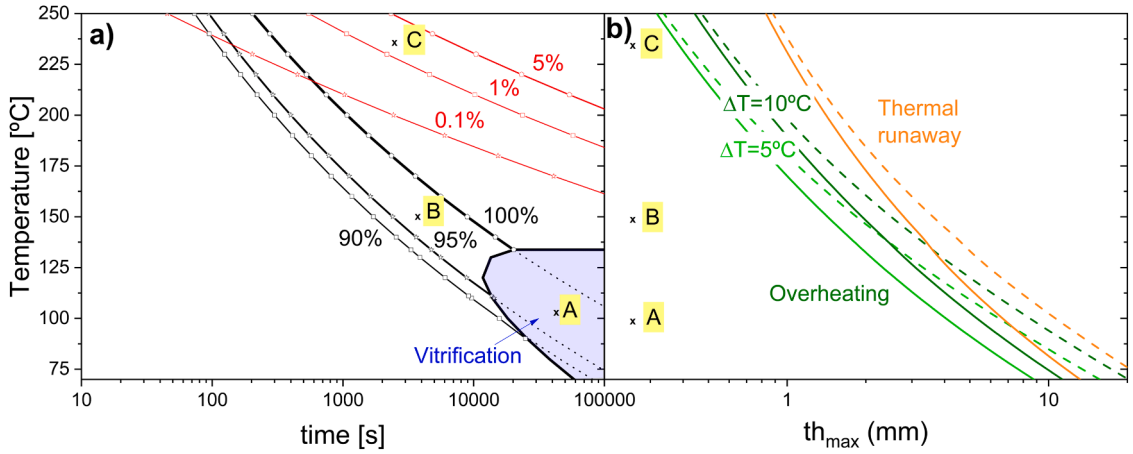


**Fig. 9.** a) Processing map of the epoxy vitrimer: Black lines show the time required to reach a 90 %, 95 % and 100 % degree of cure under isothermal conditions. Red lines show the time below which a tolerable degradation degree of 0.1 %, 1 % and 5 % is not exceeded. The blue dashed line establishes the point when curing stops progressing due to vitrification (dotted lines predicted conversion time if vitrification is neglected). b) Green lines establish the critical processable thickness above which a tolerable overheating of 5 °C (light green) and 10 °C (dark green) is exceeded. As for orange lines define the critical threshold at which the sample is expected to experience a thermal runaway (solid lines: convective heat losses are neglected ($h = 0$ in Eq. (6)); dashed lines: convection heat losses are considered ($h = 70$ W/(m2K) in Eq. (6))). (For interpretation of the references to color in this figure legend, the reader is referred to the web version of this article.)

overheating, Eq.. (7), above which the reaction becomes unstable leading to a thermal runaway. A critical thickness can be determined imposing this maximum overheating as the value of $\Delta T_{max}$ in Eq. (5). Above this critical thickness the overheating overcomes the critical one and the reaction becomes unstable, i.e., when $\Delta T_{max} = \Delta T_{max,c}$ we obtain the critical thickness for a thermal runaway to occur. Therefore, to complete the diagram, we have included the processability criterion that defines the critical threshold at which the sample is expected to experience a thermal runaway. For this criterion we have also plotted both limiting conditions: $h = 0$ and $h = 70$ W/(m$^2$K).

Once all the elements of these processing maps have been presented, we illustrate their use with a particular example, i.e., given a tolerated overheating of 10 °C, the maximum processing temperature for a 2-mm-thick plate processed by infusion should not exceed 150 °C. At that temperature, a minimum accepted degree of cure of 95 % would require at least 40 min of processing time. Under these conditions, neither degradation nor vitrification are of concern.

To validate our diagrams, we have studied three samples of approximately 5 mg in weight, labeled as A, B and C (Fig. 9.a). They have been isothermally treated at different temperatures and for different times in the thermobalance. Afterwards, their glass transition temperature has been measured by DSC. Assuming that the uncured resin was spread homogeneously at the base of the thermobalance crucible, we can infer that the thickness of the treated samples lies around 0.25 mm. Within the temperature range studied, this thickness is low enough to avoid any significant overheating and, certainly, sufficiently thin to prevent a thermal runaway (Fig. 9.b). Results of the mass loss recorded and the $T_g$ obtained for each of them are summarized in Table 2. The specimen labeled as sample A has been heated at 100 °C for 10 h. As expected, no degradation was observed at this temperature. If we stick only to the kinetics of curing, this sample should have reached a degree of cure higher than 95 %. This would imply a $T_g$ in the 120 to 130 °C range (Fig. 5). Instead, the measured glass transition was only 99 °C (Fig. 10.a), very close to the expected 100 °C when considering the phenomenon of vitrification. In addition, the DSC signal shows the activation of an exothermic process once in the rubbery state (shaded area in Fig. 10.a), consistent with the reaction of the remaining uncured fraction. Sample B was heated for 60 min at 150 °C, conditions in which vitrification is not expected. Here the measured Tg of 129.5 °C (*Fig. 10.b*) is indeed within the expected temperature range for samples cured between 95 and 100 %. As in sample A, no mass loss was recorded. Finally, sample C was treated at 235 °C for 40 min, a long enough period to well guarantee curing completion. Nevertheless, at these operating temperatures, degradation kicks in and decomposing takes place. In accordance with our diagram prediction, we have recorded a mass loss of 2.3 %. Degradation had a strong impact on the Tg which, far from the 133 °C of $T_{g,\infty}$, was only as low as 114 (Fig. 10.c).

**Table 2**
Validation experiments for the processing map.

| Sample | Tiso[ °C] | time [min] | Mass loss [%] | Tg [ °C] |
|---|---|---|---|---|
| A | 100 | 6000 | 0 | 99.0 |
| B | 150 | 60 | 0 | 129.5 |
| C | 235 | 40 | 2.3 | 114.0 |

### 3.5. Reprocessing map

The primary reaction allowing the thermoforming of aromatic disulfide containing vitrimers is a thermally-activated radically-mediated mechanism [27]. Its kinetics for the studied vitrimer have already been analyzed through stress relaxation tests [11]. The analysis yielded an $E_a$ of 187 kJ/mol and a characteristic stress relaxation time at 200 °C, $\tau_{sr}$*200, of 20 s. Stress relaxation is a characteristic time-dependent behavior of vitrimers and is analyzed by applying a fixed deformation to a specimen and measuring the load required to maintain it constant. The stress relaxation time, $\tau_{sr}$, governs how fast a vitrimer can be reprocessed and has a temperature dependence that follows an Arrhenius relationship:

$$\tau_{sr}(T) = \tau_{sr,0} exp\left(\frac{E_a}{RT}\right) \quad (9)$$

Based on the kinetic study of Luzuriaga et al. [11], we generated a TTT diagram for reprocessing the vitrimer in which $\tau_{sr}$ determines the minimum thermoforming time, $\tau_T$. This is not a very restrictive criterion since $\tau_{sr}$ is the time necessary to relax just a 63.2 % of the initial stress. We have added the limits corresponding to $2\tau_{sr}$ and $3\tau_{sr}$ corresponding to 86.4 and 95 % relaxation respectively. As with processing, degradation constraints to the time and temperature of the cycle are also taken into account. Hence, the same tolerable limits of Fig. 9 have been added to Fig. 11 accounting for thermal stability.

The sample thickness affects the time needed to homogenize the temperature during heating, $\tau_h$. Therefore, assuming that a thin plate is immersed in an isothermal bath, $\tau_T$ has been calculated as the sum of

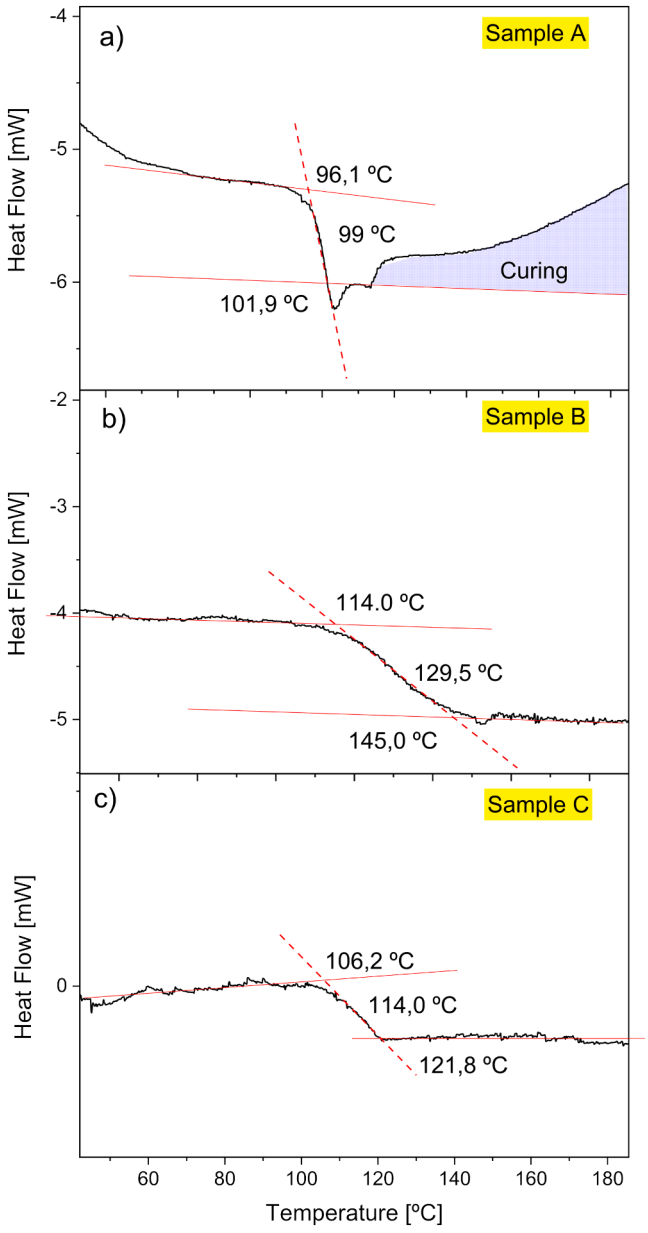


**Fig. 10.** DSC measurements of $T_g$ from samples listed in Table 2.

stress relaxation and temperature homogenization times:

$$\tau_T = \tau_{sr} + \tau_h \tag{10}$$

The following approximation has been used to calculate $\tau_h$ [59]:

$$\tau_h = \frac{\rho c_e}{k}\frac{w^2}{4}\frac{T_d - T_0}{T_s - T_0} \tag{11}$$

where $T_0$, $T_s$ and $T_d$ are the room temperature, the cycle temperature and the temperature at center of the plate, respectively. We have targeted a tolerated temperature difference ($T_s - T_d$) of 5 °C.

In Fig. 11, the lines corresponding to the minimum thermoforming time for thin plate laminates of 1, 10 and 100 mm have been plotted as dashed lines. The diagram has been restricted to isothermal reprocessing cycles ranging from 100 to 250 °C. The intersection of these lines with the tolerable degradation limits establishes the maximum thermoforming and self-healing times and temperatures. Fig. 11 shows that, while samples with thicknesses of less than 1 mm can theoretically be taken to temperatures as high as 250 °C, thicker samples must be kept at low

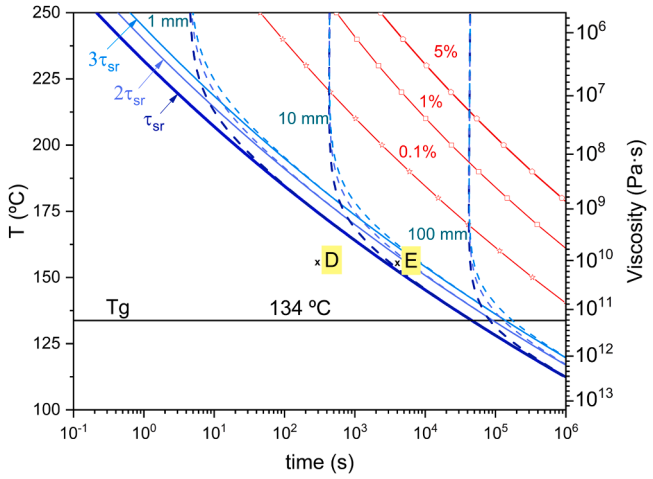


**Fig. 11.** Reprocessing map of the epoxy vitrimer: The blue solid line shows the characteristic stress relaxation time under isothermal conditions. Dashed lines set the minimum termoforming time for thin plate laminates of 1, 10 and 100 mm. Red lines show the time below which a tolerable degradation degree of 0.1 %, 1 % and 5 % is not exceeded. (For interpretation of the references to color in this figure legend, the reader is referred to the web version of this article.)

temperatures for long periods of time. We should point out that the thermal conductivity of the laminate can be significantly increased with the addition of fibers which, in turn, would reduce $\tau_h$ and consequently $\tau_T$. While considering the effects of the fiber in the reprocessing of FRP composites with vitrimer matrices is beyond the scope of this work, it would be an interesting issue to address in further studies.

In the low-temperature region, the reprocessing of vitrimers is controlled by the so-called topology freezing temperature (Tv), which sets the limit for reversible network topology through dynamic exchange. Tv is theoretically defined as the temperature at which the viscosity reaches a value of $10^{12}$ Pa·s [60]. Above this viscosity threshold, somewhat arbitrary, chemical exchanges are considered to be negligible. The established methodology for Tv measurement relies on an extrapolation of the relaxation time using the Maxwell equation and assumes a linear temperature dependency of viscosity [61–63]. This methodology yields a Tv as low as 118 °C, well below the 133 °C of $T_{g,\infty}$. When Tv is much lower than $T_g$, chain mobility is frozen in the glassy state [64]. In such a case, Tg marks the practical boundary of the vitrimer's stress relaxation behavior and, as such, has been represented in our diagram. We have completed the diagram by including a secondary *y*-axis relating viscosity to temperature. This information is useful to the extent that viscosity dictates the reprocessing techniques to be used.

To validate our diagram, we performed two experiments in which flat samples were bent and heated in a silicon bath at 155 °C (Details in Section 2.7). At this temperature, the sample is above Tv and, thus, the topological rearrangement of the vitrimer should cause a permanent

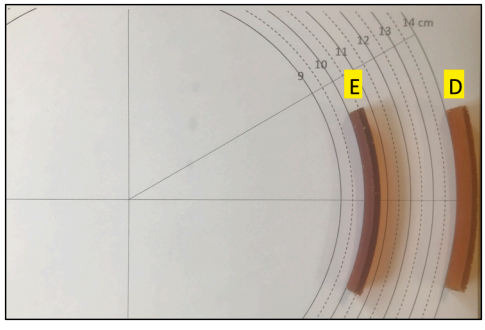


**Fig. 12.** Validation experiments for the reprocessing map.

shape change. However, it is the treatment time that will ultimately determine the success at thermoforming. Sample D was kept at this temperature for only 5 min. According to Fig. 11, not enough time to thermalize and relax the stresses. On the contrary, sample E was heated for 1 hour, i.e., well above the characteristic relaxation time of the vitrimer. Fig. 12 shows the final shapes of the two specimens after treatment. While sample E approximately kept the same radius of curvature of the tooling (100 mm), sample D has a much bigger final radius (140 mm). Therefore, indicating that in the latter, a significant part of the deformation has returned as elastic strain. These results not only support our reprocessing map, but also highlight the need to establish clear criteria for reprocessing. Let us note that, when shaping the vitrimer in a mold, it was enough to exceed the least restrictive criterion ($\tau_{sr}$) in order to achieve a large degree of deformation. However, it is highly unlikely that this reprocessing time would be sufficient for the so-called "self-healing", a process that requires high pressures and, in addition to stress relaxation, involves the kinetics of other mechanisms that we did not considered [65].

## 4. Conclusions

A complete thermal characterization along with the determination of the conditions for avoiding thermal gradients during the curing and reprocessing of thin vitrimer plates has led to the creation of processing and reprocessing maps for an aromatic disulfide-based vitrimer. Although the study was carried out for a purely resin plate, these types of diagrams could be easily applied to the case of laminates containing fibers (glass, carbon, etc.). To do so, one only has to change the overheating and thermal runaway conditions by choosing the appropriate specific heat and thermal conductivity properties of the composite. The main findings of this work are listed below: Eq. (3)-(4), Eq. (9)-(11)

- The curing process was characterized via DSC, obtaining an enthalpy of 416 kJ/mol and an apparent activation energy that varies along the process within 55 to 70 kJ/mol. We have also shown that $T_g$ changes with $\alpha$ can be fitted to the DiBenedetto equation with a $\lambda$=0.4, a $T_{g,\infty} = -26$ °C and a $T_{g,\infty}$=133 °C.
- Thermogravimetric experiments showed that, upon heating in air, the studied vitrimer undergoes a two-step decomposition process related to degradation first and combustion later. FTIR-EGA analysis of the volatiles released during the low-temperature decomposition step reveals that the thermal stability of the resin is determined by the stability of the disulfide hardener. As for degradation kinetics, an apparent activation energy in the range of 150 to 220 kJ/mol for the early stages of the decomposition ($\alpha$<0.1) was determined.
- Analytical criteria for overheating in combination with kinetic studies allowed for a refined TTT diagram to be constructed which can be used to disclose the optimal heating conditions for the rapid production of vitrimer epoxy plates. Our diagram accounts for vitrification and thermal degradation and has been experimentally validated.
- We have constructed a TTT-like diagram based on stress relaxation and degradation kinetics to optimize the resin thermoforming cycle. By taking into account the temperature homogenization time, the limitations for thermoforming a resin plate have been established. We have experimentally validated our criterion.

## CRediT authorship contribution statement

**D. Sanchez-Rodriguez:** Conceptualization, Formal analysis, Investigation, Writing – original draft. **S. Zaidi:** Investigation. **Y. Jahani:** Investigation. **A. Ruiz de Luzuriaga:** Resources, Writing – review & editing. **A. Rekondo:** Resources, Writing – review & editing. **P. Maimi:** Funding acquisition, Writing – review & editing. **J. Farjas:** Writing – review & editing, Supervision. **J. Costa:** Funding acquisition, Project administration, Writing – review & editing, Supervision.

## Declaration of Competing Interest

The authors declare that they have no known competing financial interests or personal relationships that could have appeared to influence the work reported in this paper.

## Data availability

Data will be made available on request.

## Acknowledgements

The authors acknowledge AMADE and the GRMT project (PID2021-126989OB-I00 financed by the MCI (Ministerio de Ciencia e Innovación), Spain). We also thank the support from the Catalan Government with 2017SGR1378. D.S.R. acknowledges the support received from the Beatriu de Pinós Programme and the Ministry of Research and Universities of the Government of Catalonia (Fellowship BP00069).

## References

[1] A. Wazeer, A. Das, C. Abeykoon, A. Sinha, A. Karmakar, Composites for electric vehicles and automotive sector: a review, Green Energy Intell. Transp. 2 (2022), 100043, https://doi.org/10.1016/j.geits.2022.100043.
[2] R. Hartono, A.H. Iswanto, T. Sucipto, K.M. Lubis, Effect of particle pre-treatment on physical and mechanical properties of particleboard made from oil palm trunk, IOP Conf. Ser. Earth Environ. Sci. 166 (2018) 657–664, https://doi.org/10.1088/1755-1315/166/1/012006.
[3] F.-L. Jin, S.-Y. Lee, S.-J. Park, Polymer matrices for carbon fiber-reinforced polymer composites, Carbon Lett 14 (2013) 76–88, https://doi.org/10.5714/cl.2013.14.2.076.
[4] M.Y. Khalid, Z.U. Arif, W. Ahmed, H. Arshad, Recent trends in recycling and reusing techniques of different plastic polymers and their composite materials, Sustain. Mater. Technol. 31 (2022), https://doi.org/10.1016/j.susmat.2021.e00382 e00382.
[5] W. Post, A. Susa, R. Blaauw, K. Molenveld, R.J.I. Knoop, A review on the potential and limitations of recyclable thermosets for structural applications, Polym. Rev. 60 (2020) 359–388, https://doi.org/10.1080/15583724.2019.1673406.
[6] D. Montarnal, M. Capelot, F. Tournilhac, L. Leibler, Silica-like malleable materials from permanent organic networks, Science 334 (2011) 965–968, https://doi.org/10.1126/science.1212648.
[7] W. Denissen, J.M. Winne, F.E. Du Prez, Vitrimers: permanent organic networks with glass-like fluidity, Chem. Sci. 7 (2016) 30–38, https://doi.org/10.1039/c5sc02223a.
[8] W. Alabiso, S. Schlögl, The impact of vitrimers on the industry of the future: chemistry, properties and sustainable forward-looking applications, Polymers 12 (2020), https://doi.org/10.3390/POLYM12081660.
[9] M. Guerre, C. Taplan, J.M. Winne, F.E. Du Prez, Vitrimers: directing chemical reactivity to control material properties, Chem. Sci. 11 (2020) 4855–4870, https://doi.org/10.1039/d0sc01069c.
[10] F.L. Jin, X. Li, S.J. Park, Synthesis and application of epoxy resins: a review, J. Ind. Eng. Chem. 29 (2015) 1–11, https://doi.org/10.1016/j.jiec.2015.03.026.
[11] A. Ruiz de Luzuriaga, G. Solera, I. Azcarate-Ascasua, V. Boucher, H.J. Grande, A. Rekondo, Chemical control of the aromatic disulfide exchange kinetics for tailor-made epoxy vitrimers, Polymer (2022) 239, https://doi.org/10.1016/j.polymer.2021.124457.
[12] A. Ruiz De Luzuriaga, R. Martin, N. Markaide, A. Rekondo, G. Cabañero, J. Rodríguez, I. Odriozola, Epoxy resin with exchangeable disulfide crosslinks to obtain reprocessable, repairable and recyclable fiber-reinforced thermoset composites, Mater. Horizons 3 (2016) 241–247, https://doi.org/10.1039/c6mh00029k.
[13] C.B. Cárdenas, V. Gayraud, M.E. Rodriguez, J. Costa, A.M. Salaberria, A.R. de Luzuriaga, N. Markaide, P.D. Keeryadath, D.C. Zapatería, Study into the mechanical properties of a new aeronautic-grade epoxy-based carbon-fiber-reinforced vitrimer, Polymers 14 (2022), https://doi.org/10.3390/polym14061223.
[14] L. Sorrentino, L. Esposito, C. Bellini, A new methodology to evaluate the influence of curing overheating on the mechanical properties of thick FRP laminates, Compos. Part 109 (2017) 187–196, https://doi.org/10.1016/j.compositesb.2016.10.064.
[15] L. Esposito, L. Sorrentino, F. Penta, C. Bellini, Effect of curing overheating on interlaminar shear strength and its modelling in thick FRP laminates, Int. J. Adv. Manuf. Technol. 87 (2016) 2213–2220, https://doi.org/10.1007/s00170-016-8613-5.
[16] A. Ruiz de Luzuriaga, N. Markaide, A.M. Salaberria, I. Azcune, A. Rekondo, H. J. Grande, Aero grade epoxy vitrimer towards commercialization, Polymers 14 (2022), https://doi.org/10.3390/polym14153180.

[17] S. Sourour, M.R. Kamal, Differential scanning calorimetry of epoxy cure: isothermal cure kinetics, Thermochim. Acta. 14 (1976) 41–59, https://doi.org/10.1016/0040-6031(76)80056-1.

[18] J. Wang, Q. Mao, Methodology based on the PVT behavior of polymer for injection molding, Adv. Polym. Technol. 32 (2012) 474–485, https://doi.org/10.1002/adv.

[19] Q. Li, X. Li, Y. Meng, Curing of DGEBA epoxy using a phenol-terminated hyperbranched curing agent: cure kinetics, gelation, and the TTT cure diagram, Thermochim. Acta. 549 (2012) 69–80, https://doi.org/10.1016/j.tca.2012.09.012.

[20] J. Šesták, Šesták–Berggren equation: now questioned but formerly celebrated—what is right: commentary on the Burnham paper on logistic equations in kinetics, J. Therm. Anal. Calorim. 127 (2017) 1117–1123, https://doi.org/10.1007/s10973-015-4998-x.

[21] R.J.J. Williams, M.A. Benavente, R.A. Ruseckaite, M.S. Churio, H.G. Hack, Criteria for selecting cure cycles in autoclave processing of graphite/epoxy composites, Polym. Eng. Sci. 30 (1990) 1140–1145, https://doi.org/10.1002/pen.760301805.

[22] D.J. Michaud, A.N. Beris, P.S. Dhurjati, Curing behavior of thick-sectioned RTM composites, J. Compos. Mater. 32 (1998) 1273–1295.

[23] C. Leistner, S. Hartmann, D. Abliz, G. Ziegmann, Modeling and simulation of the curing process of epoxy resins using finite elements, Contin. Mech. Thermodyn. 32 (2020) 327–350, https://doi.org/10.1007/s00161-018-0708-9.

[24] D. Sánchez-Rodríguez, H. Eloussifi, J. Farjas, P. Roura, M. Dammak, Thermal gradients in thermal analysis experiments: criterions to prevent inaccuracies when determining sample temperature and kinetic parameters, Thermochim. Acta 589 (2014) 37–46, https://doi.org/10.1016/j.tca.2014.05.001.

[25] J. Farjas, D. Sanchez-Rodriguez, S. Zaidi, D.-R.-C. Cârstea, Y. Jahani, P. Maimi, J. Costa, A. Rotrau, Analytical prediction of the curing overheating and overshoot. Application to a commercial epoxy, Submitted to, J. Therm. Anal. Calorim. (2023).

[26] Y.L. Jiun, C.T. Tze, U. Moosa, M.A. Tawawneh, Effects of recycling cycle on used thermoplastic polymer and thermoplastic elastomer polymer, Polym. Polym. Compos. 24 (2016) 735–740, https://doi.org/10.1177/096739111602400909.

[27] I. Azcune, I. Odriozola, Aromatic disulfide crosslinks in polymer systems: self-healing, reprocessability, recyclability and more, Eur. Polym. J. 84 (2016) 147–160, https://doi.org/10.1016/j.eurpolymj.2016.09.023.

[28] S.F. Gayot, C. Bailly, T. Pardoen, P. Gérard, F. Van Loock, Processing maps based on polymerization modelling of thick methacrylic laminates, Mater. Des. (2020) 196, https://doi.org/10.1016/j.matdes.2020.109170.

[29] C.K. Tziamtzi, K. Chrissafis, Optimization of a commercial epoxy curing cycle via DSC data kinetics modelling and TTT plot construction, Polymer (2021) 230, https://doi.org/10.1016/j.polymer.2021.124091.

[30] J. Mangialetto, R. Verhelle, G. Van Assche, N. Van Den Brande, B. Van Mele, Time-temperature-transformation, temperature-conversion-transformation, and continuous-heating-transformation diagrams of reversible covalent polymer networks, Macromolecules 54 (2021) 412–425, https://doi.org/10.1021/acs.macromol.0c02491.

[31] J. Farjas, P. Roura, Isoconversional analysis of solid-state transformations: a critical review. Part III. Isothermal and non isothermal predictions, J. Therm. Anal. Calorim. 109 (2012) 183–191, https://doi.org/10.1007/s10973-011-1642-2.

[32] A.S.T.M. International, Standard test method for assignment of the glass transition temperatures by differential scanning calorimetry, ASTM Int 08 (2008) 1–4.

[33] American Society for Testing and Materials, E1269-01 Standard test method for determining specific heat capacity by differential scanning calorimetry, ASTM 14 (2001), https://doi.org/10.1520/E1269-11.2. E 1269–01.

[34] S. Vyazovkin, N. Sbirrazzuoli, Mechanism and kinetics of epoxy-amine cure studied by differential scanning calorimetry, Macromolecules 29 (1996) 1867–1873, https://doi.org/10.1021/ma951162w.

[35] S. Vyazovkin, A.K. Burnham, L. Favergeon, N. Koga, E. Moukhina, L.A. Pérez-Maqueda, N. Sbirrazzuoli, ICTAC Kinetics Committee recommendations for analysis of multi-step kinetics, Thermochim. Acta. 689 (2020), 178597, https://doi.org/10.1016/j.tca.2020.178597.

[36] M. Stanko, M. Stommel, Kinetic prediction of fast curing polyurethane resins by model-free isoconversional methODS, Polymers 10 (2018) 698, https://doi.org/10.3390/polym10070698.

[37] J. Wan, C. Li, Z.Y. Bu, C.J. Xu, B.G. Li, H. Fan, A comparative study of epoxy resin cured with a linear diamine and a branched polyamine, Chem. Eng. J. 188 (2012) 160–172, https://doi.org/10.1016/j.cej.2012.01.134.

[38] M.A. Bashir, Cure kinetics of commercial epoxy-amine products with iso-conversional methods, Coatings (2023) 13, https://doi.org/10.3390/coatings13030592.

[39] L. Luo, X. Guo, Z. Zhang, M. Chai, M.M. Rahman, X. Zhang, J. Cai, Insight into pyrolysis kinetics of lignocellulosic biomass: isoconversional kinetic analysis by the modified friedman method, Energy Fuels 34 (2020) 4874–4881, https://doi.org/10.1021/acs.energyfuels.0c00275.

[40] S. Rasi, P. Roura-Grabulosa, J. Farjas, Application of thermal analysis and kinetic predictions to YBCO films prepared by chemical solution deposition methods, J. Therm. Anal. Calorim. 142 (2020) 2077–2086, https://doi.org/10.1007/s10973-020-10103-4.

[41] W. Press, B. Flannery, S. Teukolky, W. Vetterling, Numerical Recipes in C: The Art of Scientific Computing, Cambridge University Press, Cambridge, 1994.

[42] Frank-Kamenetskii DA, Diffusion and Heat Exchange in Chemical Kinetics, 2nd ed., Princeton University Press, New Jersey, 1955.

[43] A.G. Merzhanov, A.E. Averson, The present state of the thermal ignition theory: an invited review, Combust. Flame 16 (1971) 89–124, https://doi.org/10.1016/S0010-2180(71)80015-9.

[44] P.R. Ciriscioli, Q. Wang, G.S. Springer, Autoclave curing — comparisons of model and test results, J. Compos. Mater. 26 (1992) 90–102, https://doi.org/10.1177/002199839202600106.

[45] T.A. Bogetti, J.W. Gillespie, Two-dimensional cure simulation of thick thermosetting composites, J. Compos. Mater. 25 (1991) 239–273, https://doi.org/10.1177/002199839102500302.

[46] T.E. Twardowski, S.E. Lin, P.H. Geil, Curing in thick composite laminates: experiment and simulation, J. Compos. Mater. 27 (1993) 216–250, https://doi.org/10.1177/002199839302700301.

[47] T. Boddington, P. Gray, D.I. Harvey, Thermal theory of spontaneous ignition: criticality in bodies of arbitrary shape, Philos. Trans. R. Soc. London. Ser. A 270 (1971) 467–506, https://doi.org/10.1098/rsta.1971.0087.

[48] L. Sorrentino, L. Tersigni, A method for cure process design of thick composite components manufactured by closed die technology, Appl. Compos. Mater. 19 (2012) 31–45, https://doi.org/10.1007/s10443-010-9179-2.

[49] J. Farjas, P. Roura, Exact analytical solution for the Kissinger equation: determination of the peak temperature and general properties of thermally activated transformations, Thermochim. Acta 598 (2014) 51–58, https://doi.org/10.1016/j.tca.2014.10.024.

[50] J.A.G. Ruiz, J. Farjas, N. Blanco, J. Costa, M. Gascons, Assessment of unexplored isoconversional methods to predict epoxy-based composite curing under arbitrary thermal histories, J. Reinf. Plast. Compos. (2022), https://doi.org/10.1177/07316844221145591, 07316844221145591.

[51] S. Vyazovkin, N. Sbirrazzuoli, Isoconversional kinetic analysis of thermally stimulated processes in polymers, Macromol. Rapid Commun. 27 (2006) 1515–1532, https://doi.org/10.1002/marc.200600404.

[52] D. Santiago, X. Fernández-Francos, X. Ramis, J.M. Salla, M. Sangermano, Comparative curing kinetics and thermal-mechanical properties of DGEBA thermosets cured with a hyperbranched poly(ethyleneimine) and an aliphatic triamine, Thermochim. Acta 526 (2011) 9–21, https://doi.org/10.1016/j.tca.2011.08.016.

[53] N. Areny, O. Konuray, X. Fernàndez-Francos, J.M. Salla, J.M. Morancho, X. Ramis, Time-temperature-transformation (TTT) diagram of a dual-curable off-stoichiometric epoxy-amine system with latent reactivity, Thermochim. Acta 666 (2018) 124–134, https://doi.org/10.1016/j.tca.2018.06.012.

[54] D. Santín, O. Konuray, X. Fernàndez-Francos, X. Ramis, Kinetics analysis and simulation of sequential epoxy dual-curing systems with independent thermal activation, Thermochim. Acta 673 (2019) 158–168, https://doi.org/10.1016/j.tca.2019.01.023.

[55] A.T. Dibenedetto, L. Dilandro, Correlation of glass transition temperature and molecular weight: a model based on the principle of corresponding states, J. Polym. Sci. Part B 27 (1989) 1405–1417, https://doi.org/10.1002/polb.1989.090270703.

[56] M. Javdanitehran, D.C. Berg, E. Duemichen, G. Ziegmann, An iterative approach for isothermal curing kinetics modelling of an epoxy resin system, Thermochim. Acta 623 (2016) 72–79, https://doi.org/10.1016/j.tca.2015.11.014.

[57] J.P. Pascault, R.J.J. Williams, Relationships between glass transition temperature and conversion - analyses of limiting cases, Polym. Bull. 24 (1990) 115–121, https://doi.org/10.1007/BF00298330.

[58] V. Antonucci, M. Giordano, K.T. Hsiao, S.G. Advani, A methodology to reduce thermal gradients due to the exothermic reactions, Int. J. Heat Mass Transf. 45 (2002) 1675–1684, https://doi.org/10.1016/S0017-9310(01)00266-6.

[59] J.R. Welty, C.E. Wicks, W.R. E, No Title, in: N.Y. Wiley (Ed.), Fundam. Momentum, Heat Mass Transf, 1984.

[60] M. Capelot, M.M. Unterlass, F. Tournilhac, L. Leibler, Catalytic control of the vitrimer glass transition, ACS Macro Lett. 1 (2012) 789–792, https://doi.org/10.1021/mz300239f.

[61] M. Guerre, C. Taplan, R. Nicolaÿ, J.M. Winne, F.E. Du Prez, Fluorinated vitrimer elastomers with a dual temperature response, J. Am. Chem. Soc. 140 (2018) 13272–13284, https://doi.org/10.1021/jacs.8b07094.

[62] Y. Nishimura, J. Chung, H. Muradyan, Z. Guan, Silyl ether as a robust and thermally stable dynamic covalent motif for malleable polymer design, J. Am. Chem. Soc. 139 (2017) 14881–14884, https://doi.org/10.1021/jacs.7b08826.

[63] G. Lopez, L. Granado, G. Coquil, A. Lárez-Sosa, N. Louvain, B. Améduri, Perfluoropolyether (PFPE)-based vitrimers with ionic conductivity, Macromolecules 52 (2019) 2148–2155, https://doi.org/10.1021/acs.macromol.8b02493.

[64] B. Krishnakumar, R.V.S.P. Sanka, W.H. Binder, V. Parthasarthy, S. Rana, N. Karak, Vitrimers: associative dynamic covalent adaptive networks in thermoset polymers, Chem. Eng. J. 385 (2020), 123820, https://doi.org/10.1016/j.cej.2019.123820.

[65] L. An, Q. Shi, C. Jin, W. Zhao, T.J. Wang, Chain diffusion based framework for modeling the welding of vitrimers, J. Mech. Phys. Solids. (2022) 164, https://doi.org/10.1016/j.jmps.2022.104883.